

Low temperature synthesis of α -Al₂O₃ films by high-power plasma-assisted chemical vapour deposition

This article has been downloaded from IOPscience. Please scroll down to see the full text article.

2010 J. Phys. D: Appl. Phys. 43 325202

(<http://iopscience.iop.org/0022-3727/43/32/325202>)

View [the table of contents for this issue](#), or go to the [journal homepage](#) for more

Download details:

IP Address: 193.190.193.2

The article was downloaded on 02/08/2010 at 15:26

Please note that [terms and conditions apply](#).

Low temperature synthesis of α -Al₂O₃ films by high-power plasma-assisted chemical vapour deposition

Kaiyun Jiang¹, Kostas Sarakinos^{1,2}, Stephanos Konstantinidis^{1,3} and Jochen M Schneider¹

¹ Materials Chemistry (MCh), RWTH Aachen University, D-52074 Aachen, Germany

E-mail: jiang@mch.rwth-aachen.de

Received 13 April 2010, in final form 4 July 2010

Published 29 July 2010

Online at stacks.iop.org/JPhysD/43/325202

Abstract

In this study, we deposit Al₂O₃ films using plasma-assisted chemical vapour deposition (PACVD) in an Ar–H₂–O₂–AlCl₃ atmosphere. A novel generator delivering approximately 4 times larger power densities than those conventionally employed in PACVD enabling efficient AlCl₃ dissociation in the gas phase as well as a more intense energetic bombardment of the growing film is utilized. We demonstrate that these deposition conditions allow for the growth of dense α -Al₂O₃ films with negligible Cl incorporation and elastic properties similar to those of the bulk α -Al₂O₃ at a temperature of 560 ± 10 °C.

(Some figures in this article are in colour only in the electronic version)

1. Introduction

Among the various Al₂O₃ (alumina) polymorphs, the thermodynamically stable α -Al₂O₃ phase exhibits exceptional physical properties such as high hardness [1], transparency over a wide range of wavelengths [2, 3], chemical inertness and thermal stability [1, 3, 4]. Due to these properties, α -Al₂O₃ films are widely employed in surface protection and microelectronics applications. In the industrial practice, α -Al₂O₃ is grown by thermal chemical vapour deposition (CVD). A common feature of CVD-grown α -Al₂O₃ is that substrate temperatures in the excess of 1000 °C are necessary to provide the film-forming species with the energy required for α -Al₂O₃ phase formation [5]. These high deposition temperatures may cause the build-up of thermal stresses as well as interface reactions [5] and may thus lead to poor adhesion, and thermally induced crack formation and growth [6]. Furthermore, the metallurgical properties of the substrate material may be altered by substrate heating, severely limiting the choice of substrate materials. An alternative way to provide energy to the growing film and decreasing the temperature

limit for the deposition of α -Al₂O₃ is by bombardment of energetic species which are available in plasma based physical and CVD techniques. For instance, Wallin *et al* [7] demonstrated the deposition of α -Al₂O₃ on hard metal substrates at a temperature as low as 650 °C using high-power pulsed magnetron sputtering, while Takamura *et al* [8] obtained this phase at a temperature of ~500 °C employing filtered cathodic arc. Jin *et al* [9] reduced the temperature limit further for the growth of α -Al₂O₃ down to 280 °C by depositing Al₂O₃ films on Cr₂O₃ seed layer by rf magnetron sputtering. Kyrylov *et al* [10] demonstrated the growth of α -Al₂O₃ at 560 °C by plasma-assisted chemical vapour deposition (PACVD).

In all the above cases, and despite the substantial decrease in the temperature limit for the α -Al₂O₃ formation, the deposited films have been found to exhibit porosity [11, 12] and hence inferior elastic properties [12] compared with bulk and CVD α -Al₂O₃ [13]. In the case of films deposited by bipolar pulsed PACVD, Snyders *et al* [11] suggested that the porosity is caused by chlorine (Cl) incorporation into the films, due to the insufficient disassociation of the AlCl₃ precursor employed during PACVD. It is known that an increase in the plasma density can also intensify the interaction of the plasma with the gas molecules and the growing film. The plasma density in turn depends on the power applied to the discharge. The PACVD discharges available so far have been operating at voltages of

² Present address: Plasma and Coatings Physics Division, IFM Material Physics, Linköping University, SE-581 83, Linköping, Sweden.

³ Present address: Laboratoire de Chimie Inorganique et Analytique, Université de Mons, Av. Copernic 1, 7000 Mons, Belgium.

up to 0.9 kV [11, 12, 14], resulting in discharge power densities in the range from 2 to 5 W cm^{-2} . In this study we have utilized a pulsed plasma generator which is able to deliver voltages up to 1.4 kV allowing for approximately 4 times larger power densities than those achieved in the conventional PACVD processes. Using plasma characterization tools and plasma modelling we show that increasing the discharge power density values from 5 to 19 W cm^{-2} results in an increase in the energy and the flux of the bombarding species towards the growing film, as well as in a more efficient AlCl_3 dissociation. These conditions allow for the growth of dense and phase pure $\alpha\text{-Al}_2\text{O}_3$ films with negligible Cl incorporation and elastic properties close to the bulk values at a temperature of $560 \pm 10^\circ\text{C}$.

2. Experimental

Films were deposited in a semi-industrial parallel plate PACVD chamber from PLATEG GmbH. The plasma was generated by applying unipolar voltage pulses (up to 1.4 kV in amplitude) with a nominal width in the range from 80 to $100 \mu\text{s}$ and a frequency of 5 kHz on two 16 cm in diameter steel electrodes. The substrates (Si (100) wafers) were placed on the cathode, while the other electrode (anode) was grounded. The power was supplied by a pulse generator developed by Ganciu *et al* at Materia Nova R&D centre [15, 16]. The experiments were performed in an $\text{AlCl}_3\text{-Ar-H}_2\text{-O}_2$ atmosphere at a pressure of 175 Pa. The composition of the gas atmosphere was 1.2% AlCl_3 , 14.8% Ar, 82.6% H_2 and 1.4% O_2 . The substrate temperature was kept at 560°C using an external wall heating unit. The time dependent voltage and current signals were measured using an ELDITEST GE 8115 voltage and Tektronik A6303 current probe, respectively, and recorded with a Tektronik TDS 3014B digital oscilloscope. To investigate the effect of the deposition conditions on the plasma composition, *in situ* optical emission spectroscopy (OES) was employed. The OES measurements were performed using a PLASUS apparatus equipped with a charge-coupled device (CCD) camera for fast spectrum acquisition. The optical fibre was assembled together with a collimating lens to an observation window located at the chamber wall 10 mm above the cathode. The emission lines' intensities corresponding to Ar (750.4 nm), H (434.0 nm), Al (396.1 and 394.4 nm) and AlCl (261.4 nm) neutral species and Ar^+ ions (476.4 nm) were sampled through a quartz window. The phase composition of the Al_2O_3 films was determined by means of grazing incidence x-ray diffractometry (GIXRD) in a SIEMENS D5000 apparatus using a step size of 0.01° and an angle of incidence of 1° . Energy dispersive x-ray spectroscopy (EDX) measurements were carried out to determine the chemical composition of the deposited films. Scanning electron microscopy (SEM) was employed to study the influence of the deposition parameters on the film morphology, topography and thickness. Both EDX and SEM measurements were performed in a JEOL JSM-6480 apparatus, while for the EDX measurements an EDAX Genesis2000 detector was used. The elastic modulus and hardness of the as-deposited films were measured by nanoindentation. The measurements were carried out using

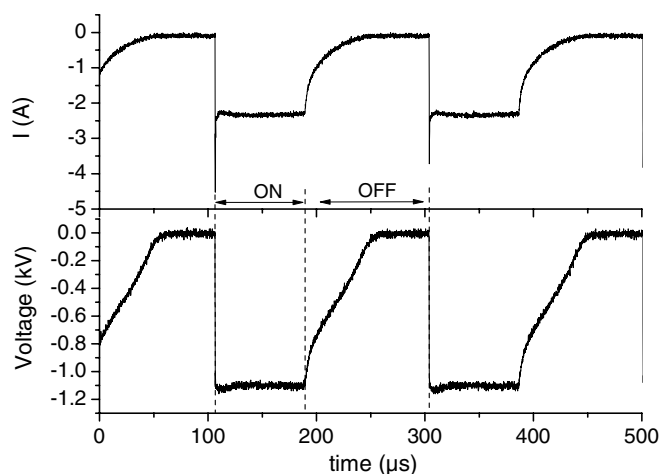


Figure 1. Time-dependent cathode voltage (bottom panel) and current (top panel) of a discharge operating at a pulse width of $80 \mu\text{s}$ and a frequency of 5 kHz.

a Berkovich tip in a Hysitron nanoindentation system. The maximum load was $2500 \mu\text{N}$ to keep the contact depth $\leq 80 \text{ nm}$. The film thickness was $\geq \sim 1.0 \mu\text{m}$. The recorded data were analysed using the method of Oliver and Pharr [17].

3. Results and discussion

Measurements of the time dependent current (I) and voltage (U) of a discharge operating at a pulse width of $80 \mu\text{s}$ and a frequency of 5 kHz are shown in figure 1. Both current and voltage exhibit constant values during the nominal pulse on-time ($80 \mu\text{s}$). As the pulse is switched off, current and voltage decay over approximately $70 \mu\text{s}$ towards zero. In the following text the magnitudes of current and voltage refer to the values measured during the pulse on-time. The I - U curve of a discharge operating at a pulse width of $80 \mu\text{s}$ and a frequency of 5 kHz is presented in the inset in figure 2. The increase in the voltage results in a close to linear increase in the current in the voltage range from 0.5 to 1.4 kV. The vertical dotted line (inset in figure 2) separates the previously studied current-voltage range [10, 11, 18] from the range investigated here. The extension of the voltage range from 0.9 kV up to 1.4 kV results in power densities (calculated by dividing the power to the area of the cathode) up to 19 W cm^{-2} , which are approximately 4 times larger than those previously reported [10, 11, 18].

The increase in the power density affects the plasma composition, as determined from the OES data shown in figure 2. The emission intensity of all lines increases as the discharge voltage and hence the cathode power density are increased. This may be consistent with an increase in the electron density and/or temperature, since the line intensity is proportional to the number density of excited atoms which in turn is related to the number density of the considered atoms in their ground states and to the density of the energetic particle responsible for the excitation. For instance, the energetic particle can be either an electron or an argon metastable atom (Ar^*). As the voltage is increased, it is reasonable to assume that electrons will acquire more energy from the applied electric field resulting in more efficient dissociation and

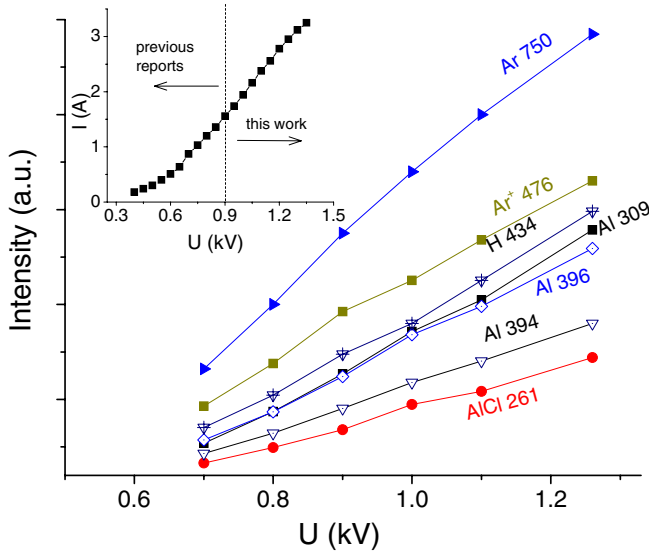
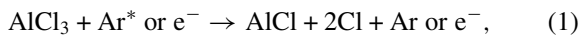


Figure 2. The intensity of the various emission lines versus the discharge voltage. The inset shows current–voltage curves recorded from the discharge operating the pulse width of 80 μ s and frequency of 5 kHz.

ionization of the plasma species. As reported in figure 2, the line intensity of the Ar 750 nm line versus the applied voltage increases. The low energy level of this transition is related to the 3P₀ and 3P₂ metastable levels of the argon atom. Hence it is reasonable to assume that the increase in the line intensity indicates an increased population of metastable Ar (Ar*) as the discharge voltage is increased. Consequently, more Ar* would be available for dissociating the precursor. Zheng *et al* reported that in an inductively coupled discharge, the presence of Ar* leads to efficient AlCl₃ precursor dissociation [19]. Generally, these dissociation processes can be described by the following reaction [19]:



which leads to the formation of Al through the reaction



Therefore, the increase in the emission intensity of precursor-related Al and AlCl lines in figure 2 should not only be attributed to the electron temperature and density increase, but also to the enhancement of the dissociation by impact of Ar*. Enhanced dissociation of BCl₃ has also been reported upon increasing the discharge power in a PACVD plasma [20].

Apart from its effect on the plasma composition, the increase in the cathode voltage to 1.3 kV leads to an up to 2 times larger discharge current as compared with the 0.9 kV discharge, as shown in the inset in figure 2, increasing the ion flux impinging on the growing film surface. In addition, the increase in the voltage implies a larger potential drop across the cathode sheath which in turn has implications for the energy of the ions impinging on the film. Due to the relatively high pressure of the discharge (175 Pa), ion–neutral and ion–electron collisions occur in the sheath [21]. Hence, the average ion energy is lower than the energy that can

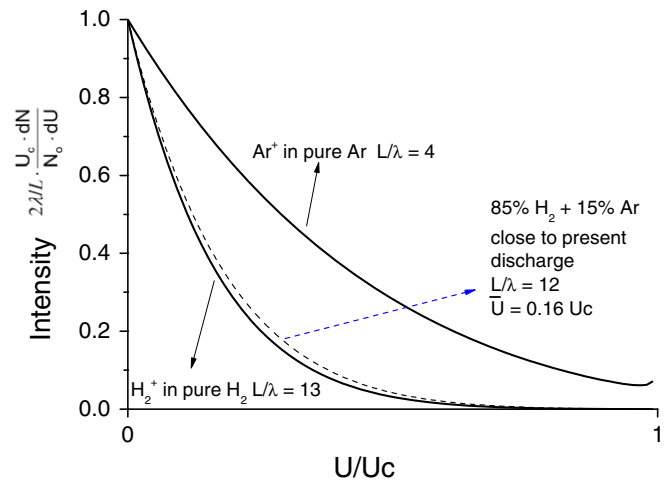


Figure 3. IEDFs for pure Ar and H₂ plasmas (solid lines) and a plasma consisting of 85% H₂ and 15% Ar (dashed line).

be gained by acceleration across the cathode fall. The ion energy distribution function (IEDF) was estimated based on the Davis and Vanderslice model [21] considering charge-exchange collisions in the sheath. The IEDF is then given by the following expression:

$$2\lambda/L \cdot \frac{U_c \cdot dN}{N_0 \cdot dU} = \frac{1}{2\sqrt{1-U/U_c}} \cdot \exp[-L/\lambda \cdot (1-\sqrt{1-U/U_c})], \quad (3)$$

where L/λ is the ratio between sheath thickness and mean free path for charge exchange collisions, N_0 is the total number of ions at the sheath edge and U_c is the potential difference across the sheath, i.e. the cathode potential. Here we evaluated for simplicity an Ar–H₂ plasma with a pressure of 175 Pa; since Ar and H₂ constitute $\sim 97\%$ of the gas atmosphere IEDFs were calculated using equation (3) for pure Ar and H₂ plasmas and plotted in figure 3 (solid lines). For the calculation of λ in equation (3), the cross sections for Ar–Ar⁺ (3×10^{-15} cm²) and H₂–H₂⁺ (8×10^{-16} cm²) charge exchange collisions were employed for Ar and H₂ plasma, respectively [22, 23]. The sheath thickness L was estimated based on the Child–Langmuir law to be 1 mm and 8 mm for Ar plasma and H₂ plasma, respectively [24]. The dashed curve in figure 3 corresponds to a plasma that consists 85% of H₂ and 15% of Ar and obtained by averaging the data from the H₂ and Ar plasma IEDFs using the respective weighting coefficients 0.85 and 0.15. These conditions are close to our experimental plasma conditions and show that the IEDF exhibits a low-populated high-energy tail starting from energies that correspond to a value $1/3U_c$, while the majority of the species exhibit energies that correspond to values below $1/4U_c$. Furthermore, the average ion energy determined by integration of the IEDF gives a value $= 0.16U_c$. Therefore, as U_c is increased from 0.9 to 1.3 kV the mean average ion energy increases from ~ 140 to ~ 200 eV. The increase in the energy and the flux of the ions towards the growing film surface results in a more intense energetic bombardment.

In figure 4, the XRD patterns of films grown at various cathode potentials are presented. At 0.9 kV cathode potential

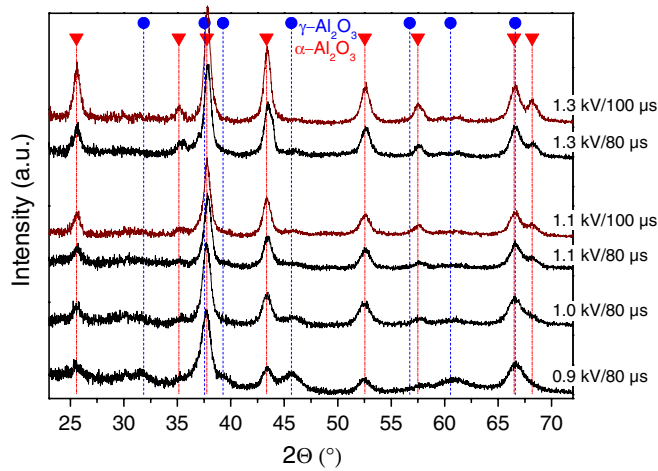


Figure 4. X-ray diffraction patterns of Al_2O_3 films deposited at various discharge voltages and pulse widths. The inverse triangles and the circles indicate the positions of the diffraction peaks associated with the presence of α - and γ - Al_2O_3 , respectively.

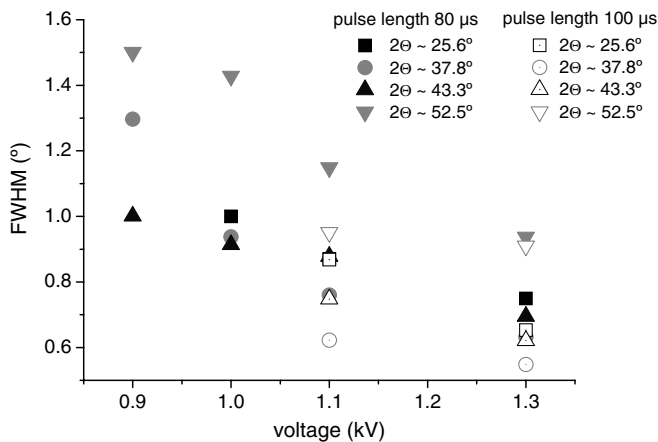
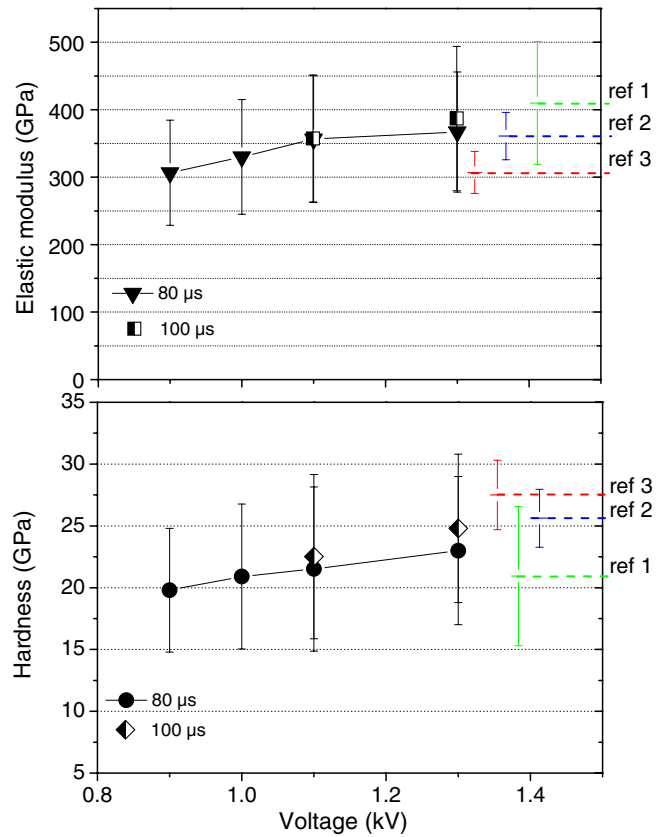


Figure 5. FWHM of chosen diffraction peaks as a function of various discharge voltages and pulse widths. Due to difficulty of peak fitting, data from sample deposited at 0.9 kV/80 μs at $2\theta \sim 25.6^\circ$ are not shown.

the formation of a mixture of γ - and α - Al_2O_3 is observed. As the voltage is increased to 1.1 kV, phase pure α - Al_2O_3 films are obtained. The increase in the voltage enhances the crystallinity of the α - Al_2O_3 phase as manifested by the decrease in the full width at half maximum (FWHM) of the XRD peaks. As shown in figure 5, FWHM values of peaks at 2θ angular positions of 25.6° , 37.8° , 43.3° and 52.5° , obtained by Gaussian fitting, show a decrease by 30–50%, when discharge voltage increases from 0.9 to 1.3 kV. Meanwhile, a clear appearance/separation of peaks at 2θ positions of 35.1° and 68.2° is also observed in figure 4 at a voltage of 1.1 and 1.3 kV, also indicating improved crystal quality. Furthermore, an increase in the pulse width from 80 to 100 μs (demonstrated for voltages of 1.1 and 1.3 kV in figure 4) leads to a decrease in the FWHM of the α - Al_2O_3 peaks by 5–10% (see figure 5) and subsequently to an improved crystallinity. The α - Al_2O_3 formation and improvement of crystallinity thereof can be attributed to the increased average ion energy as discussed in the previous paragraph as well as to the increase in duration of ion bombardment enabling



- [1] Bulk nanocrystalline α - Al_2O_3 [27]
- [2] CVD α - Al_2O_3 film[26]
- [3] RF sputtering α - Al_2O_3 film[28]

Figure 6. Elastic modulus (upper) and hardness (lower) of Al_2O_3 films as a function of the discharge voltage.

surface diffusion [10, 13, 18, 25]. It has to be mentioned here that due to the high plasma density at the voltage and pulse width of 1.3 kV and 100 μs , respectively, the substrate temperature was $590 \pm 10^\circ\text{C}$ although no external heating was applied. The deposition temperature for all other films was $560 \pm 10^\circ\text{C}$.

Along with the change in the phase composition and the improvement of the crystallinity, a continuous decrease in the Cl incorporation from 1.1 to 0.5 at% is observed as the voltage is increased from 0.9 to 1.3 kV. This may be understood by considering recently published Cl desorption data by Snyders *et al* [11] where Cl release from α -alumina films was measured during annealing at temperatures larger than the deposition temperature. This indicates that desorption of Cl may also be expected during deposition as the energy at the surface of the growing film is increased, for example, due to enhanced ion bombardment. Cl desorption during growth in turn results in a decreased Cl concentration in the film, which is again consistent with the experimental observation. Recently published *ab initio* data [11] clearly indicated that the presence of Cl destabilizes α alumina, which underlines the novelty of the here reported process where the Cl concentration could be decreased by an increase in the energy and the flux of the bombarding species towards the growing film, as well as in a more efficient AlCl_3 dissociation. As the discharge voltage is

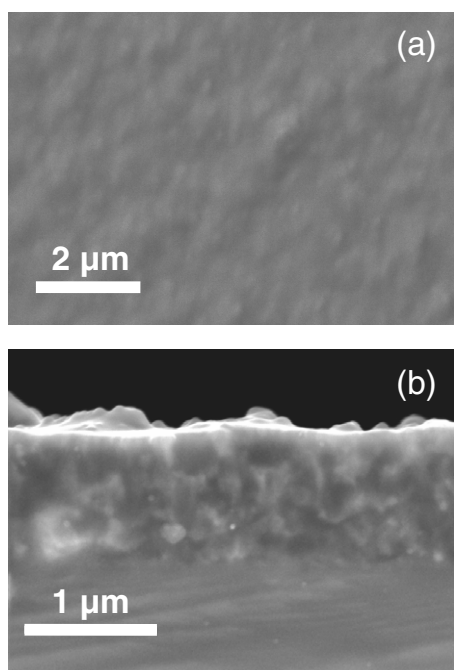


Figure 7. A top view (a) and a cross section (b) SEM micrograph from a film deposited at a discharge voltage of 1.3 kV and a pulse width of 100 μs .

increased, the Cl incorporation is reduced and the formation of the $\alpha\text{-Al}_2\text{O}_3$ phase is observed. Similar behaviour is also obtained for the films grown at a pulse width of 100 μs . At the same time the deposition rate was found to decrease from 0.5 $\mu\text{m h}^{-1}$ at a voltage of 0.9 kV to 0.36 $\mu\text{m h}^{-1}$ at a voltage of 1.3 kV (pulse width of 80 μs in both cases) which could be associated with the increase in resputtering and density of deposited film at elevated voltage. On the other hand, the change in the pulse width from 80 to 100 μs had no measurable implications for the deposition rate. The elastic modulus (E) and hardness (H) of the deposited films are plotted versus the voltage in figure 6. The quantities E and H increase as the voltage is increased. The highest values for E (~ 380 GPa) are obtained for the films synthesized at a voltage of 1.3 kV and are very similar to that of CVD grown $\alpha\text{-Al}_2\text{O}_3$ [26] and bulk ceramic $\alpha\text{-Al}_2\text{O}_3$ [27] as indicated by the horizontal dashed lines in figure 6. A top view (a) and a cross sectional (b) SEM micrographs of this film are presented in the figures 7(a) and (b), respectively. These images show a smooth surface and a dense morphology, which can be understood by the formation of phase pure $\alpha\text{-Al}_2\text{O}_3$ with a density close to the bulk value, which is a consequence of ion bombardment at elevated cathode voltage, which is characterized by both a larger flux and larger average ion energy as compared with conventional PACVD synthesis approaches.

4. Conclusions

In conclusion, we have employed a novel generator that allows for the operation of a PACVD discharge at approximately 4 times larger power density than those utilized conventionally. Plasma analysis and modelling indicate that the larger

discharge power density enables a significant increase in AlCl_3 precursor dissociation efficiency as well as an increased ion flux towards the growing film. These conditions enable the deposition of smooth and dense $\alpha\text{-Al}_2\text{O}_3$ films with negligible Cl incorporation and elastic properties similar to those of the bulk $\alpha\text{-Al}_2\text{O}_3$ at a growth temperature of $560 \pm 10^\circ\text{C}$.

Acknowledgments

The authors acknowledge the funding from the Deutsche Forschungsgemeinschaft (DFG) within Collaborative Research Centre (TFB) 289. S Konstantinidis is a postdoctoral researcher at the National Fund for Scientific Research (FNRS, Belgium), and he thanks The Interuniversity Attraction Poles Programme of the Belgian Science Policy (Project ‘PSI: Fundamentals of Plasma Surface Interactions’) for the financial support.

References

- [1] Gitzen W H 1970 *Alumina as a Ceramic Material* (Columbus, OH: The American Ceramic Society)
- [2] Aguilar-Frutos M, Garcia M and Falcony C 1998 *Appl. Phys. Lett.* **72** 1700
- [3] Holm B, Ahuja R, Yourdshahyan Y, Johansson B and Lundqvist B I 1999 *Phys. Rev. B* **59** 12777
- [4] Kramer B M and Judd P K 1985 *J. Vac. Sci. Technol. A* **3** 2439
- [5] Müller J, Schierling M, Zimmermann E and Neuschütz D 1999 *Surf. Coat. Technol.* **120–121** 16
- [6] Göbel T, Menzel S, Hecker M, Bruckner W, Wetzig K and Genzel C 2001 *Surf. Coat. Technol.* **142–144** 861
- [7] Wallin E, Selinder T I, Elfving M and Helmersson U 2008 *EPL* **82** 36002
- [8] Yamada-Takamura Y, Koch F, Maier H and Bolt H 2001 *Surf. Coat. Technol.* **142–144** 260
- [9] Jin P, Xu G, Tazawa M, Yoshimura K, Music D, Alami J and Helmersson U 2002 *J. Vac. Sci. Technol. A* **20** 2134
- [10] Kyrylov O, Kurapov D and Schneider J M 2005 *Appl. Phys. A* **80** 1657
- [11] Snyders R, Jiang K, Music D, Konstantinidis S, Markus T, Reinholdt A, Mayer J and Schneider J M 2009 *Surf. Coat. Technol.* **204** 215
- [12] Kurapov D, Reiss J, Trinh D H, Hultman L and Schneider J M 2007 *J. Vac. Sci. Technol. A* **25** 831
- [13] Wallin E, Münger E P, Chirita V and Helmersson U 2009 *J. Phys. D: Appl. Phys.* **42** 125302
- [14] Täschner C, Ljungberg B, Alfredsson V, Endler I and Leonhardt A 1998 *Surf. Coat. Technol.* **108–109** 257
- [15] Ganciu M, Hecq M, Konstantinidis S, Dauchot J P, Touzeau M, de Pouques L and Bretagne J 2004 In: *World Patent* No WO 2005/090632
- [16] Ganciu M, Konstantinidis S, Paint Y, Dauchot J P, Hecq M, de Pouques L, Vasina P, Mesko M, Imbert J C, Bretagne J and Touzeau M 2005 *J. Optoelectron. Adv. Mater.* **7** 2481
- [17] Oliver W C and Pharr G M 1992 *J. Mater. Res.* **7** 1564
- [18] Konstantinidis S, Jiang K and Schneider J M 2010 unpublished
- [19] Zheng J, Sun B, Yang R, Song X B, Li X G and Pu Y K 2008 *J. Phys. Chem. B* **112** 12748
- [20] Ramos R, Cunge G, Touzeau M and Sadeghi N 2008 *J. Phys. D: Appl. Phys.* **41** 115205
- [21] Davis W D and Vanderslice T A 1963 *Phys. Rev.* **131** 219

- [22] Ecker G and Müller K G 1961 *Z. Naturf., A: Phys. Sci.* **16** 246
- [23] Dillon J A, Sheridan W F, Edwards H D and Ghosh S N 1955 *J. Chem. Phys.* **23** 776
- [24] Langmuir I 1922 *Phys. Rev.* **21** 419
- [25] Kohara T, Tamagaki H, Ikari Y and Fujii H 2004 *Surf. Coat. Technol.* **185** 166
- [26] Hochauer D, Mitterer C, Penoy M, Michotte C, Martinz H P and Kathrein M 2008 *Surf. Coat. Technol.* **203** 350
- [27] Gong J H, Peng Z J and Miao H Z 2005 *J. Eur. Ceram. Soc.* **25** 649
- [28] Andersson J M, Czigany Z, Jin P and Helmersson U 2004 *J. Vac. Sci. Technol. A* **22** 117